

VLBA OBSERVATIONS OF A SAMPLE OF NEARBY FR I RADIO GALAXIES

Chun Xu¹, Stefi A. Baum, Christopher P. O'Dea

Space Telescope Science Institute, 3700 San Martin Drive, Baltimore, MD 21218

J.M. Wrobel

National Radio Astronomy Observatory², P.O. Box O, Socorro, New Mexico 87801

J.J. Condon

National Radio Astronomy Observatory², 520 Edgemont Road, Charlottesville, Virginia 22903

chunxu@stsci.edu, sbaum@stsci.edu, odea@stsci.edu, jwrobel@nrao.edu, jcondon@nrao.edu

ABSTRACT

We observed 17 nearby low luminosity FR I radio galaxies using the NRAO Very Long Baseline Array (VLBA) at 1.67 GHz, as part of a multi-wavelength study of a complete sample of 21 sources selected by radio flux density from the Uppsala General Catalogue of Galaxies. We detected radio emission from all 17 galaxies. At a FWHM resolution of $\approx 10 \times 4$ mas, five galaxies show only an unresolved radio core, ten galaxies show core-jet structures, and two galaxies show twin-jet structures. Comparing these VLBA images with images previously obtained with the NRAO VLA, we find that all detected VLBA jets are well-aligned on parsec scales with the VLA jets on kilo parsec scales, and that the jet to counter-jet surface brightness ratios, or the *sidedness*, decreases systematically with increasing distance along the jet. We attribute the sidedness to the Doppler boosting effect and its decline to the deceleration of the jets. We show that a distribution of Lorentz factor centered near $\Gamma = 5$ can reproduce our VLBA detection statistics for core, core-jet and twin-jet sources. We also note that the luminosity per unit length, L_j , of the VLBA jets drops quickly with distance, r , along the jet, approximately as $L_j \propto r^{-2.0}$. We discuss three different mechanisms to explain this jet *fading*: (1) the decrease of Doppler boosting due to jet deceleration, (2) synchrotron losses, and (3) expansion losses in constant velocity but adiabatically spreading jets. Mechanisms (1) and (2) are inconsistent with the observations, while mechanism (3) is consistent with the observations provided the magnetic field lines in

¹Also at: Department of Astronomy, University of Maryland, College Park, MD 20742

²NRAO is a facility of the National Science Foundation operated under cooperative agreement by Associated Universities, Inc.

the jets are aligned perpendicular to the jet axis. This implies that the deceleration of the jets required by the Unified Scheme does not occur on the tens of parsec scales, but must occur on larger scales.

Subject headings: galaxies: active — galaxies: nuclei — galaxies: lenticular — galaxies: elliptical — galaxies: jets — radio continuum: galaxies

1. Introduction

It is now generally agreed that there exist two separate categories of Active Galactic Nuclei (AGN), namely radio-loud and radio-quiet. The former have strong radio emission and usually show extended radio structures up to Mpc scales. In contrast, the latter have only weak radio emission, being about three orders of magnitude weaker at a fixed bolometric luminosity; and tend to exhibit more compact or slightly resolved radio structures, extending only ≤ 1 kpc. Within each category there are also sub-categories. The radio-louds can be sub-classified as FR I and FR II (Fanaroff & Riley 1974; Bridle 1984). The FR Is show edge-darkened radio structures, while the FR IIs show edge-brightened radio structures. Fanaroff & Riley (1974) found that radio sources with total radio powers of less than 10^{25} W Hz $^{-1}$ at 408 MHz show almost exclusively FR I morphologies, while those with radio powers higher than 10^{27} W Hz $^{-1}$ show almost exclusively FR II morphologies. For sources with intermediate radio powers, FR I and FR II radio morphologies are found in roughly equal numbers. Some “intermediate” radio morphologies between FR I and FR II are also found to exist at those intermediate radio powers (e.g., Baum et al. 1988; Owen & Laing 1989). Zirbel & Baum (1995) also found that the difference between the core radio powers of an FR I and an FR II is roughly ten times less than the difference between their total radio powers, i.e., that FR Is have cores which are a higher fraction of their total luminosity than FR IIs.

Given the complexity of AGNs, there have been many attempts to contain the diversity under unified pictures. For example, one of the schemes suggests that FR I and BL Lacertae objects are intrinsically the same and the only difference between them is the viewing angle (e.g., Browne 1983; Antonucci & Ulvestad 1985; Urry & Padovani 1995). It has also been suggested that FR Is and FR IIs have the same central engines and their differences are induced by their different environments (e.g., De Young 1993; Giovannini et al. 1994; Bicknell 1995; cf: Baum et al. 1995). The central engine in all AGNs is believed to be a super-massive black hole which accretes mass from its environment, as reviewed by Rees (1984). To disentangle the complexity of AGNs and to test different unified schemes for AGNs, systematic multi-wavelength observations of a well defined set of AGNs are necessary. We have started a series of multi-wavelength observations of a complete radio-flux-density-limited set of nearby FR I radio galaxies. The instruments we employed to date include the NRAO VLBA, the NRAO VLA, HST, and ROSAT.

Our sample consists of 21 galaxies drawn from a catalog of radio-loud galaxies constructed by Condon & Broderick (1988, hereafter CB88). That catalog was based on position coincidence of

radio identifications in the Green Bank 1400 MHz sky images (Condon & Broderick 1985, 1986; CB88) and galaxies in the Uppsala General Catalogue of Galaxies (Nilson 1973, hereafter referred to as UGC). The 21 galaxies selected for our study satisfy the following criteria: (1) Hubble type E or S0, (2) recession velocity $v_{rec} < 7000 \text{ km s}^{-1}$ (corresponds to 93 Mpc for $H_0 = 75 \text{ km s}^{-1} \text{ Mpc}^{-1}$), (3) optical major axis diameter $> 1'$, (4) total flux density S at 1400 MHz $> 150 \text{ mJy}$, (5) declination $-5^\circ \leq \delta \leq 82^\circ$, (6) having a “monster” rather than “starburst” energy source as discerned from the IRAS/radio flux ratio (CB88), and (7) a radio size $\geq 10''$ as measured from VLA images at 1.49 GHz with $2''$ resolution (Wrobel, Condon, & Machalski, in preparation), where the size is measured at contours of three times the image noise levels. The complete sample of 21 galaxies is listed in Table 1. In this paper we present the results from the VLBA observations. The HST images are presented by Verdoes et al. (1999). Throughout this paper we adopt $H_0 = 75 \text{ km s}^{-1} \text{ Mpc}^{-1}$ and define a spectral index α as $S_\nu \propto \nu^{-\alpha}$.

We wish to emphasize that a very important feature of our project is the proximity of the sample, so useful resolutions on AGN spatial features can be achieved. The farthest source in our sample is less than 100 Mpc distant, while the closest source is about 20 Mpc away (Table 1). Therefore with the 100-milliarcssecond (mas) angular resolution of HST, we resolve scales as small as $\approx 6 \text{ pc}$ near the AGN core. The environment on these scales is directly related to the nuclear activity. For example, the radius at which Bondi accretion is initiated (Bondi 1952) is $GMm_H/kT \approx 530 \text{ pc}$ for a $10^8 M_\odot$ black hole surrounded by hot gas with temperature 10^5 K . Physically, Bondi accretion can be considered as the starting point for spherically symmetric accretion, which ultimately leads to the formation of an accretion disk. Another important AGN feature is the so-called Broad Line Region (BLR) with characteristic size about 1 pc which, depending on the source, corresponds to 10 mas or $\sim \frac{1}{10}$ of the HST resolution. The VLBA with an angular resolution of $\approx 5 \text{ mas}$ can image scales well inside a 1-pc BLR.

2. VLBA Observations and Data Analysis

Fifteen galaxies from Table 1 were observed with the VLBA (Napier et al. 1994), on 1997 April 9, and two others (UGC 00408 and UGC 01004) were observed on 1997 August 22. We did not observe four of the sample galaxies with the VLBA, because UGC 06635 lacks a VLA core, making it an unsuitable target for the VLBA; UGC 07654 (NGC 4486 = 3C 274 = M87) has been extensively studied by others (e.g., Junor & Biretta 1995); and UGC 07115 and UGC 12064 were added into our sample after the VLBA observations were proposed and completed.

The VLBA received data in dual circular polarizations. Data from four contiguous 8-MHz bands were acquired with 4-level sampling for each polarization, providing a bandwidth of 32 MHz with a center frequency of 1667.49 MHz. A coordinate equinox of 2000 was assumed. Each galaxy was observed in a phase-referencing mode (Beasley & Conway 1995), meaning that a galaxy observation of duration 2.5-3.0 minutes was preceded and followed by a 2-minute observation of a phase calibrator, identified in Table 2, and typically located about 2° from the galaxy. That table

also lists the assumed positions and, where available, the 2-D positional accuracies of the phase calibrators (Patnaik et al. 1992; Browne et al. 1998; Peck & Beasley 1998; Wilkinson et al. 1998). Observations of each galaxy were spread in time to enhance coverage in the (u,v) plane. On the first observing day, each galaxy was observed 8-14 times, yielding on-source integration times of 20-35 minutes. On the second observing day, each galaxy was observed 24 times, yielding on-source integration times of 72 minutes. On both days, data were also acquired on J0555+3948 (DA 193) and used to align the phases of the four contiguous 8-MHz bands. System temperatures and gains were used to set the amplitude scale to an accuracy of about 5%, after first applying *a priori* editing and correcting for sampler errors. The data on J0555+3948 were also used to verify the amplitude calibration. Only parallel-hand correlations were delivered and archived at the VLBA correlator. All editing, amplitude calibration, fringe-fitting, phase calibration, and imaging was done with the NRAO AIPS software.

The positions given in Table 1 for UGC 00597 (NGC 315) and UGC 07494 (NGC 4374 = 3C 272.1 = M84) are from M. Eubanks (private communication), while the position for UGC 07654 is from Ma et al. (1998); these positions carry 2-D errors of ≤ 2 mas. For the other 15 galaxies observed with the VLBA, phase-referenced images were made of the Stokes I emission. We performed elliptical Gaussian fits to the VLBA cores in the phase-referenced images, to determine the galaxy positions listed in Table 1; those phase-referenced positions carry the 2-D errors appearing in Table 2 for the appropriate phase calibrator. For adequately strong galaxies, we also performed phase and amplitude self-calibrations on the (u,v) data and made another set of images with higher dynamic ranges. Figure 1 shows the final images we obtained from the VLBA observations, at the resolutions appearing in Table 1. Three of these images (UGC 01004, UGC 01413, and UGC 08419) are phase-referenced, because the radio flux densities for these galaxies are too weak (< 10 mJy) for self-calibration. All other images in Figure 1 are self-calibrated.

For all source properties other than positions, the self-calibrated VLBA image was used where available. We performed Gaussian fits to the radio core with the FWHM fixed to the angular resolution to measure the peak core flux density, S_p . The total flux density, S_t , was measured by integration within the minimum region that encloses the whole radio structure down to the lowest significant contour level, i.e., three times the off-source noise level in the VLBA image appearing in Table 1. The results for S_p and S_t are presented in Table 3 which also lists the peak core flux density, S_P ; the total radio flux density, S_T , and the elongation position angle, PA_J , measured from VLA images presented by Condon & Broderick (1988). Note that we use subscripts in lower case for VLBA symbols and in upper case for VLA symbols.

Table 3 also lists the elongation position angles of the VLBA jets, PA_j , determined as follows. VLBA images were made with Gaussian tapers close to the sizes of minor axes of the (u,v) coverage ellipsoids and restored with circular Gaussian beams. We first determined the pixel position of the core in the image through a 2-D Gaussian fit, and then made a circular cut (a ring) centered at the core. We then made a (1-D) Gaussian fit along the cut near the jet direction to find the position angle where the intensity along the cut is maximized. The position angle of each jet was measured

at different distances from the VLBA core. Since none of the VLBA jets in our sample were found to be curved, the resultant position angles were simply averaged and are listed in Table 3. As a cross check, we used the AIPS task IMFIT on images restored with the original elliptical and with the circular Gaussian beams. We found that the elongation position angle of a VLBA jet agreed very well between the two methods.

We also measured the brightness ratios between VLBA jets and counter jets, also known as the sidedness ratio, s , by using a method similar to that employed by Laing (1996). We rotated the VLBA image restored with a circular beam through 180° about its core and then divided that rotated image by the original image. This yields a sidedness image. We have set the flux density cutoffs to be three times the noise level in order to avoid meaningless values. The sidedness ratios presented in Table 3 are the mean value over each VLBA jet, averaged within the region of the jet from 15 mas from the core to the points where both side jets fade down to three times the noise level. We consider the ratios obtained through being divided by three times the noise level as lower limits to the sidedness. If more than 50% of the sidedness ratios are lower limits, we consider the averaged value as a lower limit, as presented in Table 3. A similar analysis was performed on the VLA images, yielding the sidedness ratios, S , appearing in Table 3.

3. Results

We summarize here our main results from these VLBA observations. First, as shown in Table 3, all sources are detected in these VLBA observations. UGC 07654 is known to have VLBA jets as well. Of the 17 sources, five (30%) have unresolved radio cores, ten (60%) show core-jet structures, and two (10%; UGC 07360 and UGC 11718) show twin-jet structures. A description of individual sources in the Appendix A provides more information. Thus we show that parsec-scale jets are common in low luminosity FR Is with 12 sources with jets out of 17 sources in a complete sample of 21. Second, the flux densities in these VLBA sources are dominated by their cores, S_p . The VLBA jets, if detected, contribute a small (generally $< 20\%$) fraction of the total radio flux densities, S_t , in the VLBA images, and typically extend over ≤ 100 mas or 50 pc. Third, as long as a VLBA jet is clearly detected, it is nearly parallel to its VLA jet (Figure 2 and Table 3). If the VLA jet is double-sided while the VLBA jet is only one-sided, then the VLBA jet corresponds to the stronger side of the VLA jet. Fourth, in all cases where the measurements of sidedness are without ambiguity (e.g., where the VLBA sidedness ratio, s , is a lower limit and larger than the measured VLA sidedness ratio, S ; see Figure 3 and Table 3). Note that fewer measurements of sidedness ratio are presented in Figure 3 since some sources have radio cores only so sidedness ratios are not available), the sidedness ratios of the VLBA jets are always larger than those of the corresponding VLA jets. In the case that both sidedness ratios are lower limits, the relationships are uncertain. In UGC 07360 where twin-jet structure is detected at both VLBA and VLA scales, the relation is slightly inverted, but this result is not certain given the large errors. Our results on VLBA-VLA jet alignment and sidedness ratios are consistent with the results from a study of FR Is with more

powerful radio cores (Lara et al. 1997). Fifth, as long as a VLBA jet is clearly detected, it always shows some internal structures, i.e., knots. Comparing the radio images at different scales, we notice that the structure of the knots displays some self-similarity in their properties, i.e., the overall jet structures are similar at different scales. For example, the spacing between knots in the jets seems to scale with the resolution probed. Finally, all the VLBA jets fade quickly down to noise levels. The radio luminosity per unit length of the jets, L_j , generally declines as $L_j \propto r^{-2}$, where r is the distance along the VLBA jets from their cores. Using UGC 00597 as an example, we illustrate in Figure 4 how the jet position angle, surface brightness, and sidedness change with distance from the core, both on VLBA scales (left panels) and on VLA scales (right panels). Detailed information for individual sources can be found in Appendix A. Our results are generally consistent with those found in previous studies of individual objects (e.g., Lara et al. 1997; Cotton et al. 1999).

4. Discussion

4.1. Evidence For Doppler Boosting

The brightness distributions of the jets and counter jets are usually very asymmetric, especially at parsec scales. It has long been suggested that this asymmetry is due to the Doppler beaming effect, i.e., the two jets are intrinsically symmetric, but the brightness of the jet moving towards the observer is boosted due to the relativistic motion of the jet material, and that of the jet moving away from the observer is dimmed. The strongest evidence for this hypothesis is the detection of superluminal motion in some radio galaxies and quasars (e.g., Unwin et al. 1989). Recently, superluminal motion has been found in some FR I radio galaxies (1144+35 - Giovannini et al. 1999; NGC 315 - Cotton et al. 1999). This discovery directly supports the hypothesis of relativistic motion of the jet (assuming cosmological distances). Additional strong statistical evidence in support of the Doppler favoritism on large scales is the discovery that the stronger jet is always on the side of the less-depolarized lobe (Laing 1988; Garrington 1988). This result provides strong evidence that the brighter jet indeed points toward the observer. However, the Doppler beaming hypothesis is not the only explanation that can account for the jet to counter-jet sidedness. For example, an intrinsic difference in radio power of a pair of jets can also be the reason why we see an asymmetric or one-sided jet with VLBA observations. One such model is the flip-flop jet scenario which accounts for both the asymmetric parsec-scale jets and less asymmetric kpc-scale jets (Rudnick & Edgar 1984; Feretti et al. 1993). Our results support the Doppler favoritism hypothesis, because the one-sided VLBA jet always corresponds to the stronger side of the VLA jet and the sidedness of the VLBA jet is larger than that of the VLA jet (see also, Parma et al. 1993). These findings agree with the prediction that the jet undergoes deceleration as it propagates outwards (Bicknell 1994; Baum et al. 1997). These facts are not obviously predicted if we assume that the VLBA jet is intrinsically one-sided. For example, in the flip-flop model, whether the brighter side of the parsec jet corresponds to the brighter side of the kilo parsec jet depends on which side the parsec jet is ejected when the observations are taken.

The Doppler beaming model is also supported by the following results. We note that there are no extended structures associated with the VLBA radio cores in some of our sample galaxies: UGC 05073, UGC 07455, UGC 08419, and (possibly) UGC 12531. At large scales, their jets are more symmetric than those of the rest of our sample. If the symmetry of VLA-scale jets in these sources implies that their jets lie close to the plane of the sky, rather than that the VLA-scale jets are non-relativistic, then the lack of VLBA jets in these source is consistent with the Doppler deboosting effect. The deboosting factor is $\delta^{2+\alpha}$ where $\delta = \Gamma^{-1}(1 - \beta \cos \theta)^{-1}$ (e.g., Zensus & Pearson 1987), where δ is the jet luminosity multiplier, α is the jet spectral index, $\beta = v/c$ is the jet speed, θ is the angle between the jet and the line-of-sight, and Γ is the bulk Lorentz factor of the jet. For example, for $\Gamma \approx 5$ the jets are 60 times dimmer than their rest frame brightness, assuming a spectral index $\alpha=0.6$ and $\theta = 90^\circ$. This factor of 60 would be sufficient to make the majority of the observed VLBA jets in our sample undetectable if they were to be placed in the plane of the sky.³

We carried out calculations to simulate the above scenario, i.e., to determine how the Doppler boosting and deboosting affect the statistical properties of the observed radio structures. We generated a set of model two-sided radio sources with equal jet powers in their rest frame. The viewing angles of the two-sided sources were assumed to be randomly distributed. The logarithms of the power of radio jets at parsec scale were assumed to populate a normal distribution. The Lorentz factors, Γ , were also assumed to satisfy a normal distribution. The distances to the sources were randomly assigned to one of the distances from our sample. We also set the brightness detection limit to be $0.5 \text{ mJy beam}^{-1}$, i.e., about three times the noise level of our images. Using the above assumptions, we found that if we centered the normal distribution of the logarithm of radio jet power at 29 (i.e., $10^{29} \text{ erg s}^{-1} \text{ Hz}^{-1}$) with a standard deviation 0.5, and centered the Lorentz factor at 5.0 with standard deviation of 1.0, then we could roughly reproduce our observational results. (This value for the radio jet power corresponds to a source with observed flux density 10 mJy at a distance of 100 Mpc, similar to those in our sample [Table 3].) Specifically, we found that about 17% of the sources are expected to have two-sided jets, 55% one-sided jets, and 28% no jet, similar to our observational results (cf: Sec. 3).

Figure 5 illustrates how varying the parameters affects the statistical results. First, if we increase the width of the distribution of luminosity we find fewer core-jet structures and more twin-jet structure and core sources (panel *a*). This occurs because the Doppler effect tends to make one of the jets bright and the other one dim (panel *d*). If the instrumental detection limit lies (1) between the flux densities of the pair of jets then we see a core-jet structure, (2) below that of the weak jet then we see a twin-jet structure, or (3) above the stronger jet then we then see no jet at all. Thus, a greater breadth to the distribution of intrinsic jet luminosity implies that more jets will be placed either above or below the detection limit, with the result that fewer sources are

³The observed radio power of the jets will be equal to the intrinsic power for an angle to the line of sight of $\approx 35^\circ$ for $\Gamma \approx 5$.

observed to have a core-jet structure. Second, our results are not very sensitive to the width of the distribution of Lorentz factor (panel *b*) because an increase in Lorentz factor tends to produce more core-jet and core sources while a decrease in Lorentz factor tends to produce more twin-jet sources, so these two effects somewhat balance out. Third, an increase in the median Lorentz factor will result in more core jets and core only sources, and fewer twin-jet structures (panel *c*). This is understandable from panel *d* since a larger Lorentz factor will increase the jet-to-counter jet ratio and further deboost the jets near the plane of the sky, thereby producing more core-jet structures and more undetectable jets but fewer twin-jet sources.

4.2. Why Do the VLBA Jets Fade?

While all the sources in our sample have kpc-scale radio jets, their parsec-scale jets, if detected, all fade at a distance less than ~ 50 mas (or typically ~ 30 pc) in our VLBA images. For the sources lacking VLBA jets, it is plausible that the jets fade at an even shorter distance or are deboosted. Is the fading of the jets in the VLBA images an artifact related to the VLBA sensitivity? The VLBA sensitivity to large scale diffuse structure drops quickly at scales larger than 250 mas in our observations, which places all our observed jets well within the angular scales probed by our VLBA observations. We assume the jets are continuous since we observe the jets at larger scales and the simple evolution of the sidedness ratio with distance suggests the large scale jets are developed from the VLBA-scale jets we see here. The VLBA-scale jets in our images are laterally unresolved, as tested with Gaussian fits across the jets. Thus the fading of a VLBA-scale jet is not due to the jet's being resolved out, thus lowering the peak surface brightness. Rather, there is a real decrease of the observed jet power.

To quantify the fading of the jets, we performed a detailed analysis of the evolution in jet brightness along the well defined jets in the galaxies UGC 00597, UGC 01841, UGC 06723, and UGC 07360. We constructed diagrams of jet flux density per unit length *vs* distance along the jet. We assume that the radio structure is made of three components (an unresolved core, a jet, and a counter-jet) and we performed a nonlinear fit to the data. The basic strategy of the fit is as follows. We take a δ -function as the core, plus two components $\propto r^{-\lambda}$ as the jet and the counter jet. We then convolve these functions with a Gaussian and perform the nonlinear fit. The detailed equations for the fitting can be found in the footnote under Table 4, which lists the fitted parameters. We find values of λ ranging from 1.6 to 2.3. Jones & Wehrle (1997) presented multi-frequency VLBA observations for one of our galaxies, UGC 07360 and they found $\lambda \approx 2.0$, slightly steeper than our fitted value of 1.6. However, their analysis neglected the contamination of the jet from the core; if we fit the jet without assuming the central δ -function, we do reproduce their $\lambda \approx 2.0$.

It is worth noting that, in the above discussion, the fading of the jets only applies to scales of parsecs to tens of parsecs. At scales beyond hundreds of parsecs the jets appear to evolve differently, probably due to the interaction between the jets and the external medium. In fact, the evolutionary slope λ in UGC 06723 is about 1.0 for the jet between 100 and 400 pc (Figure 13a in Baum et al.

1997), although that slope is based on the variation of the peak jet amplitude with distance along the jet. Another interesting source is UGC 03087 (3C120), for which Walker et al. (1987) discuss radio data on the jet ranging from 0.5 pc to over 400 kpc (for $H_0 = 100$) and found an overall slope of 1.27. However, we note that in their Figure 15 the slope within 100 pc is about 2.3, steeper than its overall value and more in agreement with our results on these size scales.

The fading of the jets on parsec scales could be the result of at least three mechanisms or their combination: (1) The jet is decelerated from ultra-relativistic to intermediate relativistic speed, thereby effectively reducing the Doppler beaming effect. (2) The jet power is reduced through synchrotron losses. (3) The jet undergoes adiabatic expansion which reduces the jet internal energy. Each of these mechanisms will now be considered in turn.

4.2.1. *Doppler Boosting*

Here we consider whether the decrease in jet brightness could be caused by a reduction in Doppler boosting as an initially relativistic jet decelerates. An important observational constraint is that the two-sided and one-sided jets fade in the same manner.

According to Baum et al. (1997, 1998), the observed jet surface brightness variation satisfies

$$I_j \propto (\Gamma\beta)^{-(2\alpha+3)/3} \delta^{2+\alpha} w^{-(10\alpha+9)/3} \propto \Gamma^{-4.1} \beta^{-1.4} w^{-5.2} (1 - \beta \cos \theta)^{-2.7} \quad (1)$$

for jets with magnetic fields running parallel to the jet axis, and

$$I_j \propto (\Gamma\beta)^{-(5\alpha+6)/3} \delta^{2+\alpha} w^{-(7\alpha+6)/3} \propto \Gamma^{-5.7} \beta^{-3.1} w^{-3.5} (1 - \beta \cos \theta)^{-2.7} \quad (2)$$

for jets with magnetic fields running perpendicular to the jet axis. Hence the variation of the laterally integrated brightness goes as

$$I_j \propto \Gamma^{-4.1} \beta^{-1.4} w^{-4.2} (1 - \beta \cos \theta)^{-2.7} \quad (3)$$

for the B_{\parallel} case and

$$I_j \propto \Gamma^{-5.7} \beta^{-3.1} w^{-2.5} (1 - \beta \cos \theta)^{-2.7} \quad (4)$$

for the B_{\perp} case. Here Γ is the jet Lorentz factor, w is the transverse jet width, θ is angle to the line-of-sight, $\alpha = 0.65$ is the jet spectral index, and $\delta = \Gamma^{-1} (1 - \beta \cos \theta)^{-1}$. We calculate the jet brightness evolution for different cases, i.e., different lines of sight, different jet opening angles (with adiabatic effects taken into account) and different magnetic field configurations and the results are shown on Figure 7. The jet brightness I_j is plotted against jet velocity β where we assume that the jet is decelerated linearly with the distance from the core over these scales. (Note: since the jets are laterally unresolved, brightness I_j and luminosity per unit length L_j are linearly associated; so this plot can be considered equivalent to a plot of L_j against β and thus can be directly compared with our observational results.)

Figure 7 shows that the behavior of the jet brightness as the jets decelerate is somewhat complicated because there are two competing effects. (1) The change in the Doppler boosting factor as the jets decelerate causes the jets pointing towards us to dim and the jets pointing away from us and those near the plane of the sky to brighten. (2) The deceleration of the jet compresses the jet fluid along the jet axis and increases the jet density and the magnetic field. This causes the jets to brighten. The jets dominated by perpendicular magnetic field brighten much more than the jets dominated by parallel magnetic field since $B_{\parallel} \propto w^{-2}$ while $B_{\perp} \propto (w\beta\Gamma)^{-1}$ (Baum et al. 1997, 1998).

The fact that model jets pointed towards us evolve differently than those in the plane of the sky is inconsistent with the result that the one-sided and two-sided jets are observed to fade in the same manner. The fact that over much of the orientation range, the model jets brighten rather than dim is inconsistent with the fact that the jets are observed to fade. Thus, we can rule out the hypothesis that deceleration of an initially relativistic jet is responsible for the observed fading of the jets on the tens of pc scale.

4.2.2. *Synchrotron Losses*

Here we consider the hypothesis that synchrotron losses can account for the jet fading. These sources have equipartition magnetic fields of $\sim 5 \times 10^{-3}$ G (Table 4). Using the standard formula $t_s = 8 \times 10^8 B^{-2} \gamma^{-1}$ s to calculate the synchrotron lifetime and assuming an electron (not bulk) Lorentz factor $\gamma \sim 10^3$, which is typical for GHz radio emission in the above magnetic field, we find $t_s \sim 1000$ yr. Thus, the corresponding travel distance of an electron in the jet is about 300 pc for a jet with speed c . This value is more than 10 times the scale of fading seen in our VLBA images. However, the magnetic field could be stronger than the equipartition field on these scales. Increasing the magnetic field by a factor of 10 above equipartition reduces the electron lifetime by a factor of order 100 and the fading would thus occur on the observed scales. In fact, Venturi et al. (1993) estimated a higher value of the brightness temperature for the jets in UGC 00597 than we do, implying a higher equipartition magnetic field and thus a shorter life for synchrotron-emitting electrons. Jones & Wehrle (1997) found that the spectral indices of the jets in UGC 07360 steepen with the distance from the core, as expected for the synchrotron loss mechanism. Thus, it is possible that the fading of a VLBA jet is due simply to synchrotron losses in a magnetic field about one order of magnitude higher than the equipartition value.

We assume (1) the jet undergoes virtually no expansion, consistent with observations of M 87 on these scales (Junor et al. 1999; Junor & Biretta 1995), (2) synchrotron radiation is the dominant energy loss mechanism for the ultra-relativistic electrons, (3) the jet has constant velocity $\approx c$, and (4) constant magnetic field. The latter is justified because the sound speed of the jet is much smaller than that of light speed as implied from the brightness temperature in Table 4. The energy change of a synchrotron emitting electron satisfies $dE/dt = -\eta E^2$, where $\eta = 1.6 \times 10^{-3} B^2$ and B is the magnetic field. If we assume the distribution of synchrotron electrons is $N(E, 0) = NE^{-p}$,

where $p = (2\alpha + 1)$, we then have $N(E, t) = NE^{-p}(1 - \eta Et)^{(p-2)}$ at any later time (Kardashev 1962; Wilson 1975). Note here we have $E < 1/\eta t$, i.e., there are no electrons with energy above $1/\eta t$ because of synchrotron losses. Thus, we have

$$L_j \propto (1 - \eta Et)^{(p-2)} \propto (1 - \eta Er/c)^{(p-2)} \propto (1 - Ar)^{(2\alpha-1)} \quad (5)$$

as a result of constant jet speed, where L_j is the radio luminosity per unit length of the jets as mentioned in Sec. 3. This relationship is not a simple power-law and is effectively flatter ($\propto -r$ near the origin) than observed (Figure 6), i.e., it is not an acceptable fit to the observed jets (see Table 4). Thus, we rule out the possibility that a simple synchrotron loss model can explain the fading of the VLBA jets because (1) it would require a magnetic field an order of magnitude higher than the equipartition value and (2) the observed decline of jet brightness is inconsistent with the predicted slope.

4.2.3. Adiabatic Expansion of a Constant Velocity Jet

If adiabatic evolution is the dominant energy loss mechanism in the jet, we expect that the jet luminosity per unit length will depend on its transverse width w as $L_j \propto w^{-\lambda}$ and will depend on distance along the jet r as $L_j \propto (w_0 + 2r\Theta)^{-\lambda}$. These dependencies assume a constant jet opening angle, Θ , and constant jet velocity, β . Moreover, for an optically thin jet with spectral index 0.65, λ will be 4.2, 2.5 or 3.1, depending on whether the magnetic field runs parallel to the jet, runs perpendicular to the jet, or is maintained at the equipartition value (Jones & Wehrle 1997).

Very little data are presently available on the magnetic field structures in FR I radio galaxies on these linear scales. We note that powerful quasars tend to have magnetic fields parallel to the jets on scales of parsecs to tens of parsecs, while those in BL Lacertae objects tend to be perpendicular to the jets (Cawthorne et al. 1993; Gabuzda et al. 1994; Wardle 1998). If we assume that the current BL Lac/FR I unification schemes are correct, then the magnetic fields in FR Is should also be perpendicular to the jets. M 87 is a counter example to this extrapolation and shows magnetic field mostly parallel to the jets except at the knots (Perlman et al. 1999). This question can only be answered with polarimetry of the jets in our sample. A perpendicular magnetic field would produce an exponent of 2.5 for the variation of jet luminosity per unit length *vs* distance, which is comparable to the observed value of 2.0 (Table 4).

In summary, we find that adiabatic expansion of a constant velocity jet is consistent with the observed jet fading under the assumption that the magnetic field is perpendicular to the jet axis. This prediction should be tested with (1) VLBA polarimetry to determine the magnetic field morphologies and (2) higher resolution observations to determine whether the jets are indeed expanding. An important implication of this result is that the deceleration of these jets which is implied by the Unified Scheme does not take place on tens of pc scales, but must instead occur on larger scales (e.g., hundreds of parsecs or larger). Baum et al. (1997) showed that the properties

of the jet in 3C 264 are consistent with strong deceleration on hundreds of pc scales. Laing et al. (1999) argue for deceleration on similar or slightly larger scales in a sample of B2 radio galaxies.

5. Summary

We present VLBA observations of 17 members of a complete sample of 21 nearby FR I radio galaxies for which we also have VLA, HST, and ROSAT data. We detected parsec-scale radio emission in all 17 sources observed with the VLBA. Five VLBA sources show only a radio cores, ten sources show core-jet structures, and two sources show twin-jet structures. We find that the VLBA images are core-dominated, while the VLBA scale jets, if detected, contribute only a small fraction (mostly < 20%) of the total VLBA radio flux densities. We also find that (1) all VLBA jets are aligned with VLA jets; (2) the jet-to-counter-jet sidedness ratio measured with the VLBA is generally larger than that measured with the VLA; (3) the VLBA jets fade with distance from the AGN core as luminosity per unit length $L_j \propto r^{-2.0}$; (4) the observations suggest self-similarity in the structures of the knots. We argue that results (1) and (2) are consistent with Doppler boosting effects on the parsec scales and deceleration of the jets between scales of tens of parsecs and kilo parsecs. We show that a distribution of bulk Lorentz factors centered near $\Gamma = 5$ can reproduce our VLBA detection statistics for core, core-jet, and twin-jet sources. We consider three hypotheses to explain our result that the jets fade on the tens-of-parsecs scale. (i) If the fading is due to a decrease of the Doppler boosting as the jet decelerates, it would predict very different behavior for the one-sided and two-sided jets, contrary to observations. Also, in most cases we would expect the jets to *brighten*, not fade, due to compression of the jet fluid as the jet decelerates. (ii) Synchrotron losses in a magnetic field about an order of magnitude higher than our estimated equipartition values would produce dimming on the appropriate size scales, but with a slope to the brightness evolution which is inconsistent with the observed value. (ii) Expansion losses in an adiabatically expanding jet, with constant velocity and opening angle, are roughly consistent with the observations, provided the magnetic field structure in the jets is perpendicular to the jet axis. This should be tested with VLBA polarimetry to determine the magnetic field structure and higher resolution observations to determine the jet expansion. Our results imply that the jets do not decelerate on the tens of pc scale but must decelerate on larger scales.

C.X. is grateful for the hospitality of NRAO, would like to thank Alan Roy for help with some of the VLBA data reduction, and was partially supported by a grant from the STScI Director’s Discretionary Research Fund. We are grateful to the anonymous referee for helpful comments on the paper.

A. Comments on Individual Sources

UGC 00408 (NGC 193): The VLBA image of this source shows clear core-jet radio structure. There is also evidence for a knot with flux density 1.4 mJy, located 42.3 mas from the core at position angle 104° . This knot is thus on the jet side, yet well beyond the faded jet (Figure 1). X-ray observations using the High Resolution Imager on board the ROSAT observatory reveal that the X-ray structure of this source consists of two components: an east-west component elongated near the jet direction and lying on the optical center, plus an elliptical ring oriented north-south and matching the size of the optical galaxy (Xu et al. 2000).

UGC 00597 (NGC 315): This source has been extensively studied using the VLA and VLBI (e.g., Venturi et al. [1993], Cotton et al. [1999] and references therein). The radio jets are found to have large sidedness ratios from mas to arcmin scales.

UGC 00689 (NGC 383 = 3C 31): On the arcsec scale, this source displays an S-type symmetry and a sidedness ratio of ≥ 20 . The sidedness ratio of our VLBA image is ≥ 6 . Lara et al. (1997) measured sidedness ratios at $30''$, $15''$, and 8 mas to be 1.5, 6, and >16 , respectively, with VLA and VLBI data at 5 GHz. The spectral index of the VLBI core between 1.65 and 4.95 GHz is found to be -0.44, indicating an inverted spectrum and assuming no flux density variations between our observations on 1997 April 9 and those of Lara et al. (1997) on 1993 February 25.

UGC 01004 (NGC 541): A weak radio core was detected in this source, which may be marginally resolved in our VLBA image.

UGC 01413 (NGC 741 = 4C 05.10): This galaxy is a member of a pair of binary galaxies NGC 741/742. The VLA image displays a core residing near the center of NGC 741 plus a knot $30''$ to the east of that core (Birkinshaw & Davis 1985). Our VLBA image marginally detects a core with no obvious extended structure associated with it.

UGC 01841 (3C 66B): This source displays a C-type symmetry in its radio jets on arcmin scales (e.g., Hardcastle et al. 1996). Optical synchrotron emission associated with the radio jets has also been detected in this source (Butcher et al. 1980). Our VLBA image shows a core-jet structure (Figure 1). The lower resolution image restored with a circular Gaussian beam (cf: Sec. 2) reveals a knot at 59 mas to the north-east of the core. The latter image resembles the EVN-MERLIN image made by Fraix-Burnet et al. (1997) except that the overall scale of our image is larger, suggesting self-similarity between small and intermediate scale structure.

UGC 03695 (NGC 2329): This galaxy is a cluster member in Abell 569. It hosts a wide angle tailed radio source with the bulk of the radio emission coming from the core (Feretti et al. 1985). The VLBA detects a core-jet elongated in the direction corresponding to the northeastern radio tail.

UGC 05073 (NGC 2892): An unresolved radio core was detected in our VLBA image, with no associated extended structure. The lower limit of the core to jet flux ratio is estimated to be \sim

140.

UGC 06723 (NGC 3862 = 3C 264): The overall radio structure of this galaxy is very unusual. It consists of three structural components: a small-diameter core, a one-sided jet, and a large amorphous emission plateau (Bridle & Vallée 1981). Optical synchrotron emission is associated with the jet (Crane et al. 1993; Baum et al. 1997). Recent global VLBI and VLA images of this source can be found in Lara et al. (1997), while MERLIN images appear in Baum et al. (1997).

UGC 07360 (NGC 4261 = 3C 270): HST observations of this galaxy reveal a nuclear dust disk which is nearly perpendicular to the large scale radio jets (Jaffe et al. 1993, 1996). An enclosed mass of $\sim 4 \times 10^7 M_\odot$ within 0.1 pc was also suggested by those studies. Our VLBA image shows this source has a twin-jet structure at parsec scales. Parsec-scale twin jets have been detected in fewer than ten FR I radio sources so far (Xu et al. 1999). Parsec-scale images obtained with the VLBA at other wavelengths can be found in Jones & Wehrle (1997).

UGC 07455 (NGC 4335): This source has well-defined, two-sided jets on scales of tens of arc seconds. However, we are unable to detect any jet-like structures associated with the nearly unresolved radio core at mas scales. The VLBA core to jet flux density ratio is estimated to be greater than ~ 23 .

UGC 07494 (NGC 4374 = 3C 272.1 = M84): We detect core-jet structure in this source, with the VLBA jet pointing towards the northern and the stronger and narrower of the VLA jets.

UGC 08419 (NGC 5127): This source has quite symmetric two-sided jets on scales of tens of arc seconds. Yet the VLBA image shows no evidence for jets. The core to jet flux density ratio is estimated to be greater than about 10.

UGC 08433 (NGC 5141): Core-jet structure is detected, with the mas jet pointing to the southern and slightly stronger VLA jet.

UGC 09058 (NGC 5490): Similar to the situation in UGC 08433, a core-jet structure is detected with the mas jet pointing to the eastern and slightly stronger VLA jet.

UGC 11718 (NGC 7052): We see evidence for two-sided emission (in NNE and SSW directions) in this source at mas scales, with the stronger side pointing to the nearly one-sided jet on scales of tens of arc seconds. If confirmed, this will be a very special case of twin jets detected at VLBA scales but one jet detected at VLA scales. But we should be very cautious about the possible twin-jet structure since it could also be a symmetrization artifact due to inaccurate amplitude calibration. We are unable to perform any further tests on this feature due to its weakness. However, we still count this source as a twin-jet source because the detected twin-jet feature is well aligned with the large scale jet.

UGC 12531 (NGC 7626): We detect weak evidence for a core-jet structure in this source. The jet is misaligned by 10° from the direction of the northern VLA jet. This apparent misalignment could be a real offset between VLBA and VLA jets. However due to the faintness of the jet, the

measurement is uncertain.

REFERENCES

Antonucci, R. R. J., & Ulvestad, J. S. 1985, *ApJ*, 294, 158

Baum, S.A., Zirbel, E.L., & O'Dea, C.P. 1995, *ApJ*, 451, 88

Baum, S.A., Heckman, T., Bridle, A., van Breugel, W., & Miley, G. 1988, *ApJS*, 68, 643

Baum, S.A., et al. 1997, *ApJ*, 483, 178 (with Errata, 1998, *ApJ*, 492, 854)

Beasley, A.J., & Conway, J.E. 1995, in *ASP Conf. Ser. 82, Very Long Baseline Interferometry and the VLBA*, eds. J.A. Zensus, P.J. Diamond, & P.J. Napier (San Francisco: ASP), 327

Bicknell, G. 1994, *ApJ*, 422, 542

Bicknell, G. 1995, *ApJS*, 101, 29

Birkinshaw, M., & Davis, R.L. 1985, *ApJ*, 291, 32

Bridle, A.H., & Vallée, J.P. 1981, *AJ*, 86, 1165

Bridle, A.H. 1984, *AJ*, 89, 979

Bondi, H., 1952, *MNRAS*, 112, 195

Browne, I. W. A. 1983, *MNRAS*, 204, 23P

Browne, I.W.A., Patnaik, A.R., Wilkinson, P.N., & Wrobel, J.M. 1998, *MNRAS*, 293, 257

Butcher, H.R., van Breugel, W., & Miley, G.K. 1980, *ApJ*, 235, 749

Cawthorne, T. V., Wardle, J. F. C., Roberts, D. H., Gabuzda, D., & Brown, L. F. 1993, *ApJ*, 416, 496

Condon, J.J., & Broderick, J.J. 1985, *AJ*, 90, 2540

Condon, J.J., & Broderick, J.J. 1986, *AJ*, 91, 1051

Condon, J.J., & Broderick, J.J. 1988, *AJ*, 96, 30 (CB88)

Cotton, W. D., Feretti, L., Giovannini, G., Lara, L., & Venturi, T., 1999, *ApJ*, 519, 108

Crane, P., et al. 1993, *ApJ*, 402, L37

De Young, D. S., 1993, *ApJ*, 405, 207

Fanaroff, B.L., & Riley, J.M. 1974, *MNRAS*, 167, 31

Feretti, L., Giovannini, G., Gregorini, L., Padrielli, L., Roland, J., & Valentijn, E.A. 1985, *A&A*, 147, 321

Feretti, L., Comoretto, G., Giovannini, G., Venturi, T., & Wehrle, A.E. 1993, *ApJ*, 408, 446

Fraix-Burnet, D., Despringre, V., & Baudry, A. 1997, *Vistas in Astronomy*, 41, 237

Gabuzda, D. C., Mullan, C. M., Cawthorne, T. V., Wardle, J. F. C., & Roberts, D. H. 1994, *ApJ*, 435, 140

Garrington, S.T., Leahy, J.P., Conway, R.G., & Laing, R.A. 1988, *Nature*, 331, 147

Giovannini, G., Feretti, L., Venturi, T., Lara, L., Marcaide, J., Rioja, M., Spangler, S.R., & Wehrle, A.E. 1994, *ApJ*, 435, 116

Giovannini, G., Taylor, G. B., Arbizzani, E., Bondi, M., Cotton, W. D., Feretti, L., Lara, L., & Venturi, T., 1999, *ApJ*, 522, 101

Hardcastle, M.J., Alexander, P., Pooley, G.G., & Riley, J.M. 1996, *MNRAS*, 278, 273

Jaffe, W., Ford, H.C., Ferrarese, L., van den Bosch, F., & O'Connell, R.N. 1993, *Nature*, 364, 213

Jaffe, W., Ford, H.C., Ferrarese, L., van den Bosch, F., & O'Connell, R.N. 1996, *ApJ*, 460, 214

Jones, D.L., & Wehrle, A.E., 1997, *ApJ*, 484, 186

Junor, W., & Biretta, J.A. 1995, *AJ*, 109, 500

Junor, W., Biretta, J.A., & Livio, M., 1999, *Nature*, 401, 891

Kardashev, N.S. 1962, *Soviet Astronomy*, 6, 317

Laing, R.A. 1988, *Nature*, 331, 149

Laing, R.A. 1996, in *Energy Transport in Radio Galaxies and Quasars*, ed. P.E. Hardee, A.H. Bridle, & J.A. Zensus, *ASP Conference Series*, Vol 100, 241

Laing, R. A., Parma, P., de Ruiter, H. R., & Fanti, R., 1999, *MNRAS*, 306, 513L

Lara, L., Cotton, W.D., Feretti, L., Giovannini, G., Venturi, T., & Marcaide, J.M. 1997, *ApJ*, 474, 179

Livio, M. 1997, in *IAU Colloquium 163, Accretion Phenomena and Related Outflows*, ed. Wickramasinghe, D.T., Ferrario, L., & Bicknell, G.V., (San Francisco: *ASP Vol. 121*), 439

Ma, C., et al. 1998, *AJ*, 116, 516

Napier, P.J., Bagri, D.S., Clark, B.G., Rogers, A.E.E., Romney, J.D., Thompson, A.R., & Walker, R.C. 1994, *Proc. IEEE*, 82, 658

Nilson, P. 1973, *Uppsala General Catalogue of Galaxies* (Uppsala Astronomical Observatory, Uppsala)

Owen, F. N., & Laing, R. A. 1989, *MNRAS*, 238, 357

Parma, P., Morganti, R., & de Ruiter, H.R. 1993, *A&A*, 267, 31

Patnaik, A.R., Browne, I.W.A., Wilkinson, P.N., & Wrobel, J.M. 1992, *MNRAS*, 254, 655

Perlman, E. S., Biretta, J. A., Zhou, F., Sparks, W. B., & Macchetto, F. D., 1999, *AJ*, 117, 2185

Peck, A.B., & Beasley, A.J., 1998, in *IAU Colloquium 164, Radio Emission from Galactic and Extragalactic Compact Sources*, ed. Zensus, J.A., Taylor, G.B., & Wrobel, J.M., (San Francisco: *ASP Vol. 144*), 155

Rees, M.J. 1984, *ARA&A*, 22, 471

Reid, M.J., Biretta, J.A., Junor, W., Muxlow, T.W.B., and Spencer, R.E., 1989, *ApJ*, 336, 112

Rudnick, L., & Edgar, B.K. 1984, *ApJ*, 279,

Rudnick, L., & Edgar, B.K. 1984, ApJ, 279, 74

Unwin, S.C., Cohen, M.H., Biretta, J.A., Hodges, M.W., & Zensus, J.A. 1989, ApJ, 340, 117

Urry, C.M., & Padovani, P. 1995, PASP, 107, 803

Venturi, T., Giovannini, G., Feretti, L., Comoretto, G., & Wehrle, A.E. 1993, ApJ, 408, 81

Verdoes Kleijn, G.A., Baum, S.A., de Zeeuw, P. T., & O'Dea, C.P. 1999, AJ, 118, 2592

Walker, R.C., Benson, J.M., & Unwin, S.C. 1987, ApJ, 316, 546

Wardle, J. F. C. 1998, in IAU Colloquium 164, *Radio Emission from Galactic and Extragalactic Compact Sources*, eds. J. A. Zensus, G. B. Taylor, & J. M. Wrobel, ASP Conference Series, 144, 97

Wilkinson, P.N., Browne, I.W.A., Patnaik, A.R., Wrobel, J.M., & Sorathia, B. 1998, MNRAS, 300, 790

Wilson, A.S. 1975, A&A, 43, 1

Xu, C., O'Dea, C.P., & Biretta, J.A. 1999, AJ, 117, 2626

Xu, C., Baum, S.A., O'Dea, C.P., et al., 2000, in preparation.

Zensus, J.A., & Pearson, T.J. 1987, in *Superluminal Radio Sources*, ed. Zensus, J.A. & Pearson, 1

Zirbel, E.L., & Baum, S.A. 1995, ApJ, 448, 521

Figure Captions

Fig 1. VLBA images of Stokes I emission at 1.67 GHz from 17 FR I radio galaxies. The lowest contour levels correspond to three times the noise levels and contours are spaced at $3\sigma \times [-3, -2, -1, 1, 2, 4, 8, 16, 32, 64, 128, 256, 512]$. The images of UGC 00408, UGC 01413, and UGC 08419 are phase-referenced. All other images are self-calibrated.

Fig 2. Histogram of the position angle offsets between jets on VLBA (mas/pc) and VLA (arcsec/kpc) scales. This plot indicates that the jets at VLBA scale and those at VLA scale are very well aligned.

Fig 3. Jet sidedness at both VLBA (mas/pc) and VLA (arcsec/kpc) scales. The arrow-like bars associated with the data represent the lower/upper limits. The dashed line indicates equal jet sidedness on the VLBA and VLA scales. The fact that more points lie above the dashed line indicates that the sidedness at VLBA scales are on average larger than those at VLA scales, which further implies a deceleration of the radio jets.

Fig 4. UGC 00597. Variation of jet position angle, surface brightness, and sidedness ratio as a function of distance from the core on both VLBA (mas/pc) and VLA (arcsec/kpc) scales.

Fig 5. Panels (a), (b), and (c) indicate the fractions of sources with two detectable jets (above the open circles), only one detectable jet (between the open and filled circles), or core only (below the filled circles) as functions of (a) the standard deviation of the distribution of the jet luminosity, (b) standard deviation of the distribution of the jet bulk Lorentz factor, and (c) the mean jet bulk Lorentz factor. Panel (d) shows the Doppler boosting factors of jets (solid lines and upper curves) and counter jets (dotted lines and lower curves) as a function of viewing angle for bulk Lorentz factors 2, 3, 4, 5, and 6. The open and filled circles in panel (a), (b) and (c) were obtained through simulations and the curves running through the dots are simply fits to the simulated results. The curve for Lorentz factor equals 5 in panel (d) is plotted with a thicker line for clarity.

Fig 6. Fits to the radio jet brightness as a function of distance from the core for four sources where the VLBA jets are clearly detected. The solid points in the upper part of each plot represent observed data. The solid line is the fit to the data with a power law and the dash-dotted line is the fit with a synchrotron loss model. The solid points in the lower part of the plot represent the residuals from the power law fit and the open circles represent those from the synchrotron loss model (cf: Table 4).

Fig 7. Illustration of the predicted variation of jet brightness I_j with jet bulk velocity in a decelerating relativistic jet due to both Doppler boosting and adiabatic expansion/compression effects (see Sec. 4.2.1). The expected variations are shown for a range of line-of-sight inclination angles, three values of jet opening angle ($5^\circ, 15^\circ, 25^\circ$), and magnetic field oriented both parallel and perpendicular to the jet axis. In each plot, the curves from top to bottom corresponds to jets at line-of-sight inclination angles $5^\circ, 15^\circ, 30^\circ, 45^\circ, 60^\circ, 75^\circ, 90^\circ, 120^\circ$ and 150° , with the 90° curves plotted with a thicker line for clarity.

TABLE 1. VLBA POSITIONS, RESOLUTIONS, AND SENSITIVITIES FOR UGC GALAXIES

UGC	Other name	m_p (mag)	Hubble Type	D_{75} (Mpc)	α_{J2000}	δ_{J2000}	Resolution (mas,mas, $^{\circ}$)	Image <i>r.m.s.</i> (mJy/b.a.)
00408	NGC 193	13.9	S0	60.3	00 39 18.5829	+03 19 52.584	9.8,3.8,−6	0.10
00597	NGC 315	12.5	E	69.1	00 57 48.8834 ^a	+30 21 08.812 ^a	10.3,3.9,−7	0.11
00689	3C 31	13.6	E0	71.1	01 07 24.9593	+32 24 45.237	10.2,3.9,−7	0.12
01004	NGC 541	14.0	E	73.8	01 25 44.3078	−01 22 46.522	12.4,5.6, 0	0.10
01413	NGC 741	13.2	E	76.3	01 56 20.9902	+05 37 44.277	11.0,4.3,−5	0.16
01841	3C 66B	15.0	E	88.1	02 23 11.4073	+42 59 31.403	9.4,3.9,−8	0.13
03695	NGC 2329	13.7	E-S0	78.3	07 09 08.0061	+48 36 55.733	11.2,3.6,−10	0.13
05073	NGC 2892	14.4	E	90.8	09 32 52.9316	+67 37 02.630	10.9,3.8, 21	0.12
06635	NGC 3801	13.3	E	42.0	11 40 17.31	+17 43 36.8	—	—
06723	3C 264	14.0	E	84.9	11 45 05.0099	+19 36 22.756	10.3,4.1,−4	0.11
07115		14.4	E	89.5	12 08 05.81	+25 14 16.4	—	—
07360	3C 270	12.0	E	27.7	12 19 23.2162	+05 49 29.702	10.6,4.5,−2	0.10
07455	NGC 4335	13.7	E	63.1	12 23 01.8881	+58 26 40.384	8.0,4.4,−4	0.14
07494	M 84	10.8	S0	14.6	12 25 03.7433 ^a	+12 53 13.143 ^a	10.8,4.0,−5	0.15
07654	M 87	10.4	E	16.0	12 30 49.4234 ^b	+12 23 28.044 ^b	—	—
08419	NGC 5127	13.9	E	64.3	13 23 45.0156	+31 33 56.703	10.1,4.2,−17	0.12
08433	NGC 5141	13.9	S0	70.0	13 24 51.4403	+36 22 42.763	9.8,4.1,−19	0.12
09058	NGC 5490	13.4	E	66.2	14 09 57.2984	+17 32 43.911	10.4,4.2,−8	0.12
11718	NGC 7052	14.0	E	69.1	21 18 33.0446	+26 26 49.251	10.4,3.8,−6	0.10
12064	3C 449	14.6	E-S0	72.4	22 31 21.35	+39 21 33.2	—	—
12531	NGC 7626	12.8	E	48.3	23 20 42.5391	+08 13 00.992	11.9,5.1, 6	0.18

Notes: ^a M. Eubanks, private communication. ^b Ma et al. 1998.

TABLE 2. VLBA PHASE CALIBRATORS FOR UGC GALAXIES

UGC	Calibrator	Phase		2-D Error	
		α_{J2000}	δ_{J2000}	(mas)	Ref.
00408	J0049+0237	00 49 43.2363	+02 37 03.785	14	1,3
00597	J0112+3208	01 12 50.3276	+32 08 17.548	>55	1,3
00689	J0112+3208	01 12 50.3276	+32 08 17.548	>55	1,4
01004	J0127+0158	01 27 22.8822	+01 58 24.534	14	3
01413	J0201+0343	02 01 51.5093	+03 43 09.256	14	1,3
01841	J0230+4032	02 30 45.7068	+40 32 53.087	12	1,2
03695	J0710+4732	07 10 46.1052	+47 32 11.142	12	1,2
05073	J0903+6757	09 03 53.1559	+67 57 22.683	12	1,2
06723	J1148+1840	11 48 37.7776	+18 40 08.983	14	1,3
07360	J1222+0413	12 22 22.5501	+04 13 15.780	14	1,3
07455	J1217+5835	12 17 11.0203	+58 35 26.228	12	1,2
07494	J1213+1307	12 13 32.1412	+13 07 20.373	—	1
08419	J1329+3154	13 29 52.8650	+31 54 11.047	55	1,4
08433	J1317+3425	13 17 36.4935	+34 25 15.923	55	1,4
09058	J1412+1334	14 12 36.3728	+13 34 38.166	14	1,3
11718	J2114+2832	21 14 58.3340	+28 32 57.206	55	1,4

References: 1. Peck & Beasley 1998. 2. Patnaik et al. 1992. 3. Browne et al. 1998. 4. Wilkinson et al. 1998.

TABLE 3. SOURCE PROPERTIES IN THE VLBA (1.67 GHz) AND VLA (1.49 GHz) IMAGES

UGC	VLBA Flux Density		VLA Flux Density		Morphology ^a		Position Angle		Sidedness Ratio	
	Peak	Total	Peak	Total	VLBA	VLA	VLBA	VLA	VLBA	VLA
	S_p	S_t	S_P	S_T			PA_j	PA_J	s	S
00408	29.8±0.5	36.6±0.6	40±0.9	145±1.7	CJ	CJ	101	92	>3	>7
00597	223.7±19.0	356.0±24.0	396±2.1	501±2.4	CJ	CJ	-50	-49	>25	>4
00689	44.1±1.5	51.6±1.6	89±1.4	198±2.1	CJ	TJ	-18	-21	>6	>20
01004	1.9±0.4	2.7±0.4	8±0.8	33±1.6	C	CJ	—	-104	—	—
01413	4.4±0.6	8.6±0.8	13±1.0	104±2.8	C	CJ	—	—	—	—
01841	112.0±5.0	157.4±6.0	131±12.0	510±24.0	CJ	CJ	50	50	>25	>20
03695	49.7±1.6	59.1±1.8	117±2.2	271±3.3	CJ	CJ	-30	-29	>3	—
05073	15.3±0.6	17.5±0.6	22±0.7	94±1.4	C	TJ	—	52	—	~1.5
06635	—	—	—	1032±21.0	—	TJ	—	115	—	~1.8
06723	122.9±6.1	166.1±7.1	386±9.3	848±14.0	CJ	CJ	30	25	>12	>8
07115	—	—	—	41±2.0	—	CJ	—	116	—	>2.5
07360	67.4±9.3	160.4±14.0	165±1.0	173±1.1	TJ	TJ	-93	-96	~1	~1.5
07455	9.2±0.5	10.9±0.5	15±1.5	115±4.2	C	TJ	—	79	—	~1.0
07494	106.0±1.6	119.0±1.7	112±13.0	2254±58.0	CJ	TJ	1	0	>5	~1.5
07654	1570.0	—	3600±200	56090±150	CJ	CJ	-84 ^b	-70 ^b	> 200 ^c	>15
08419	3.9±0.5	5.2±0.6	7±0.7	41±1.7	C	TJ	—	118	—	~1.0
08433	35.3±2.0	43.8±2.2	71±2.7	859±9.4	CJ	TJ	-168	-170	>3	~1.5
09058	20.0±1.0	25.5±1.1	41±7.0	403±22.0	CJ	TJ	75	75	>2	~1.0
11718	27.9±0.9	32.1±1.0	36±0.9	98±1.5	TJ	CJ	-157	-158	>2	—
12064	—	—	—	18±1.1	—	TJ	—	11	—	—
12531	12.5±0.6	15.4±0.7	23±1.0	128±0.4	CJ	TJ	44	32	>1.5	~1.0

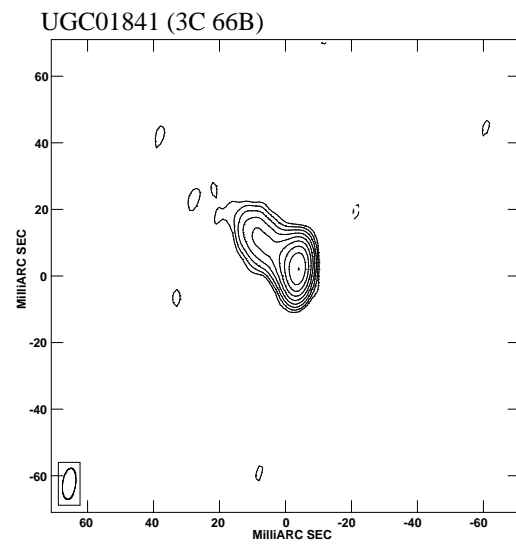
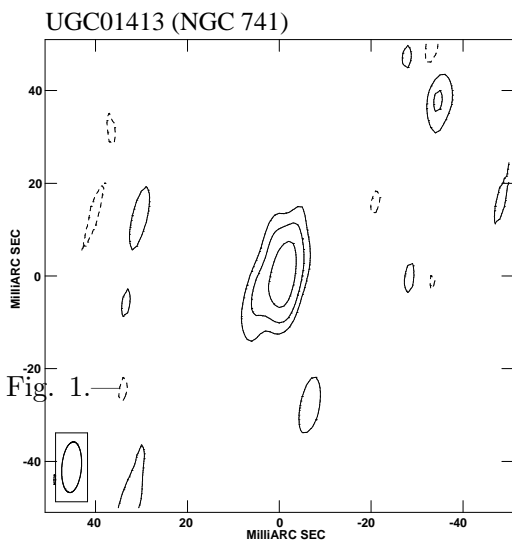
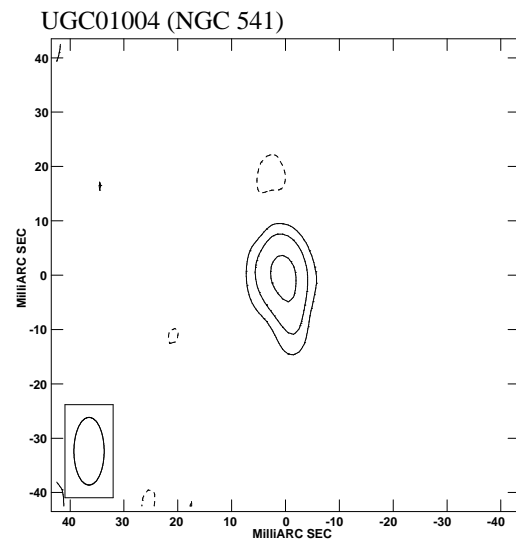
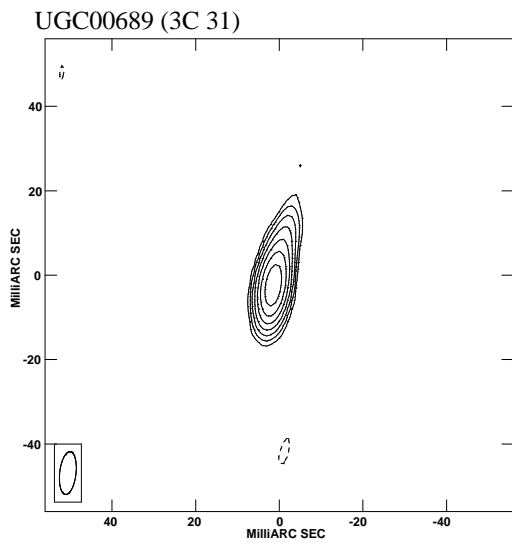
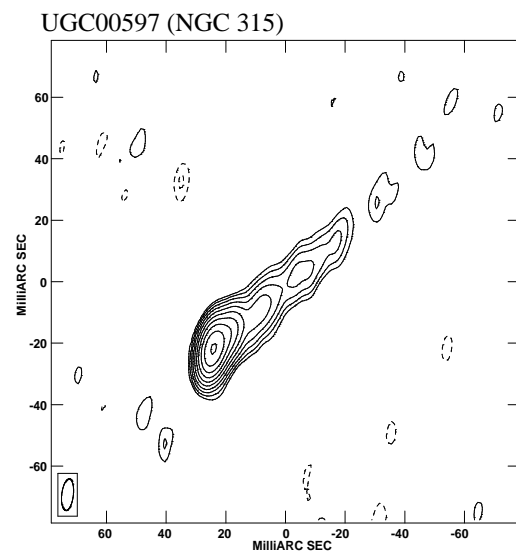
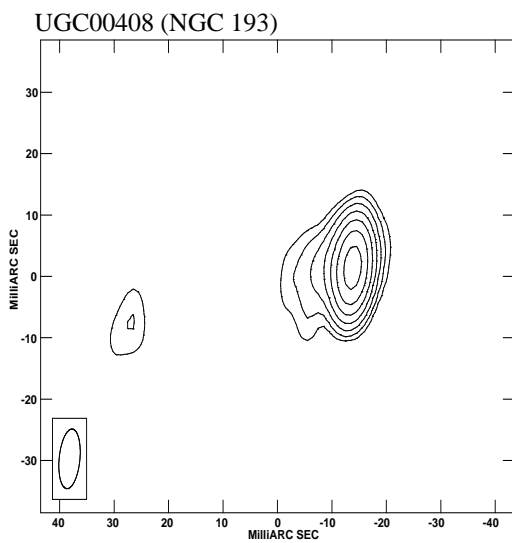
Notes: ^a C means core, CJ means core-jet, TJ means twin-jet. ^b Values from Junor & Biretta 1995.

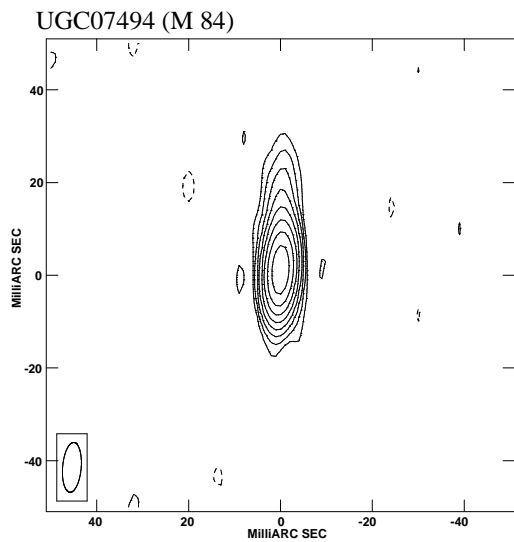
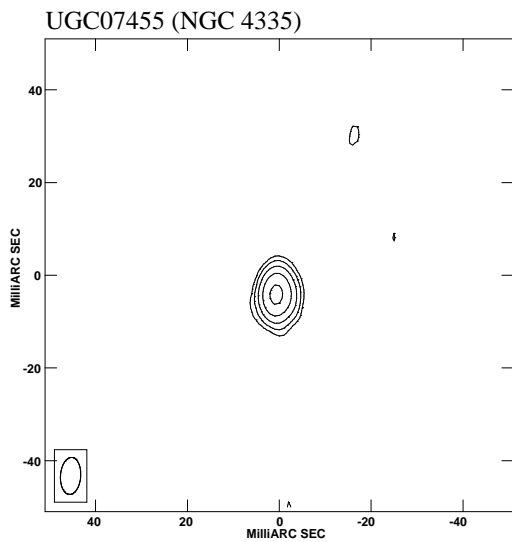
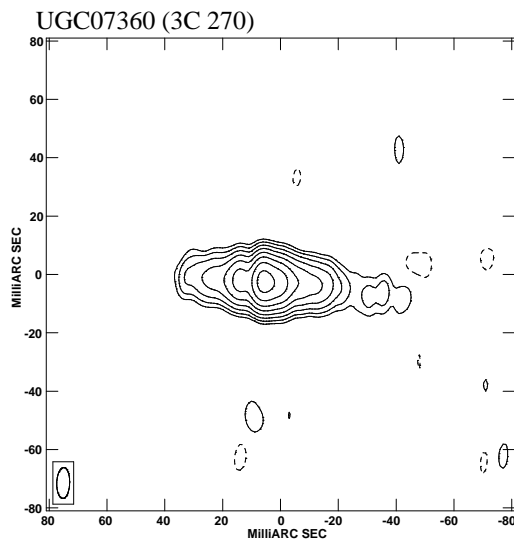
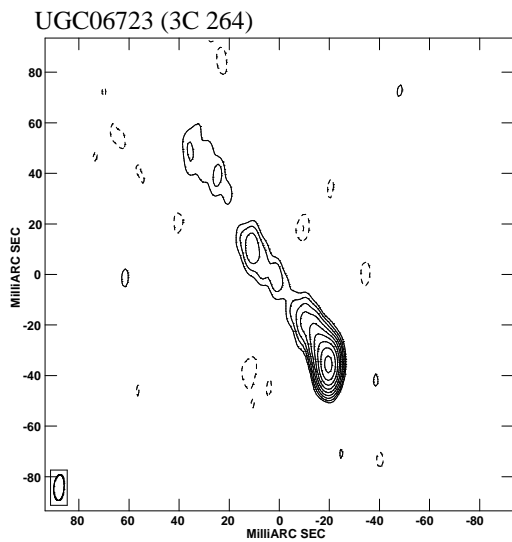
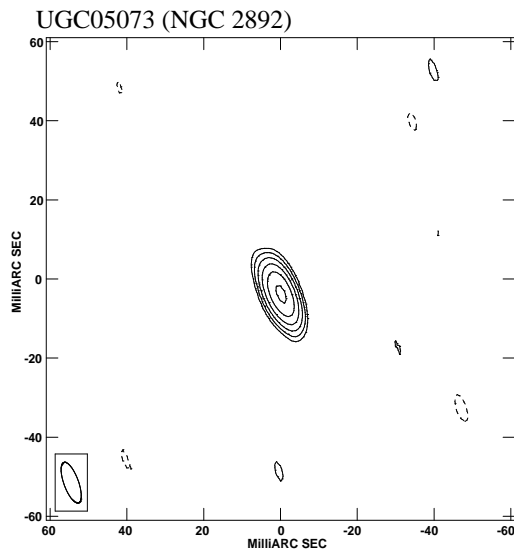
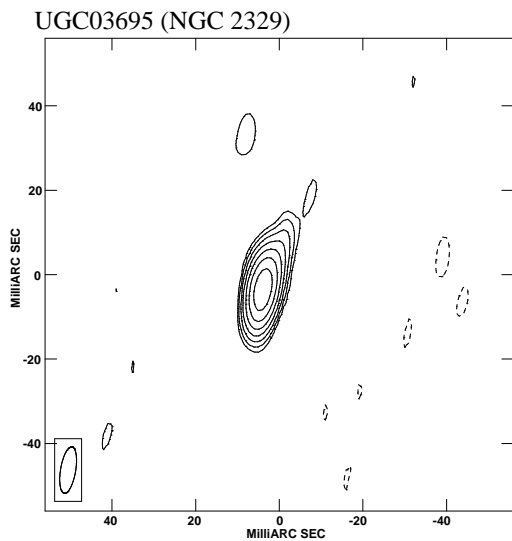
^c Values from Reid et al. 1989. VLBA and VLA values are denoted by lower case and upper case subscripts, respectively.

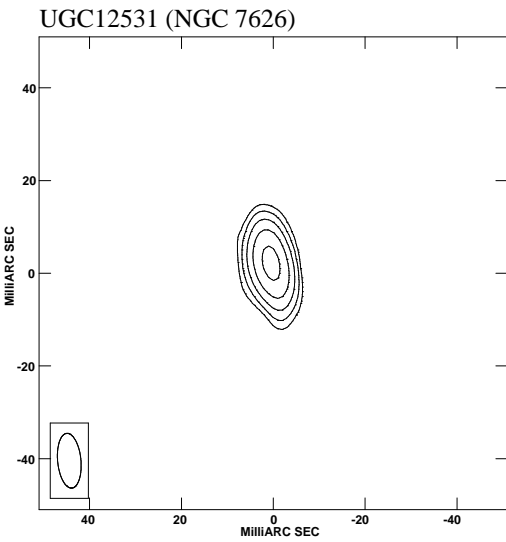
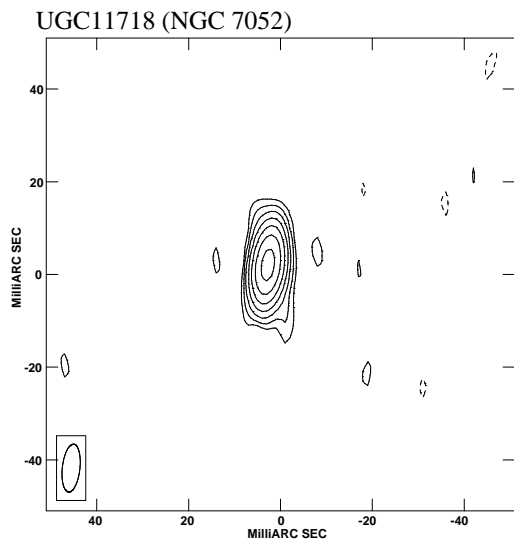
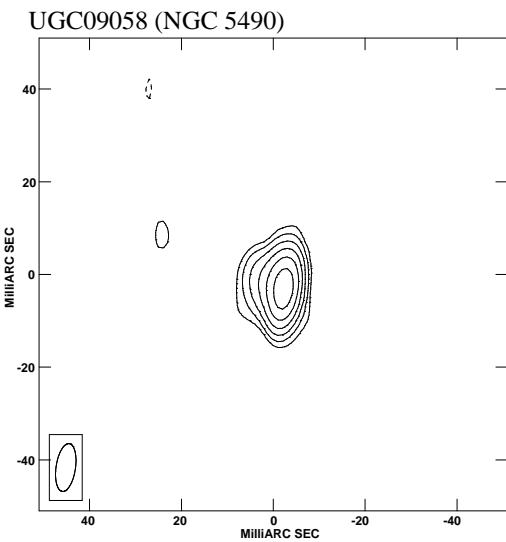
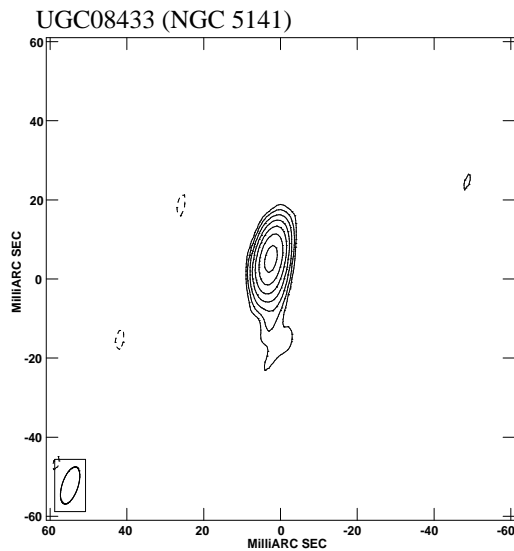
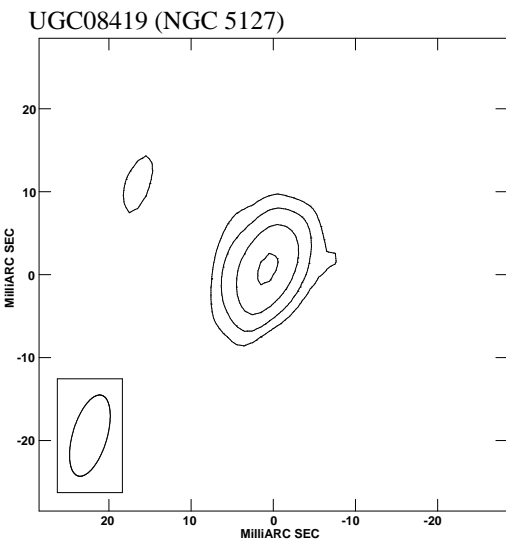
TABLE 4. FITS TO VLBA JET EVOLUTION

UGC	A_1	A_2	A_3	λ	T_b (K)	B_{eq} (G)	χ_p^2	χ_s^2
00597	34.3	97.4	18.6	2.1	8.2×10^7	6.6×10^{-3}	9.9	150
01841	16.6	41.9	3.6	2.2	4.5×10^7	5.5×10^{-3}	4.4	100
06723	17.1	67.6	9.4	2.3	3.8×10^7	5.3×10^{-3}	3.9	33
07360	11.4	16.7	13.5	1.6	5.6×10^7	6.0×10^{-3}	6.9	145

Explanation: The Table presents the results of the fit (cf: Fig 6) of the jet surface brightness evolution to the function $(A_1\delta(r) + A_2r^{-\lambda} + A_3(| - r|)^{-\lambda})$ convolved with $\frac{1}{\sqrt{2\pi}\sigma}e^{-\frac{r^2}{2\sigma^2}}$, where A_1 , A_2 , and A_3 correspond to the core, jet, and counter jet strengths, respectively, in arbitrary units; and σ is fixed according to the FWHM angular resolution. Values of χ^2 are given corresponding to the power law fit, χ_p^2 , and the synchrotron loss model, χ_s^2 . T_b is the jet brightness temperature and B_{eq} is the equipartition magnetic field in the jet both estimated between 15 and 20 mas from the core, in order to avoid contamination by the core. Since the jets are unresolved laterally, a jet width of 1 pc is assumed.







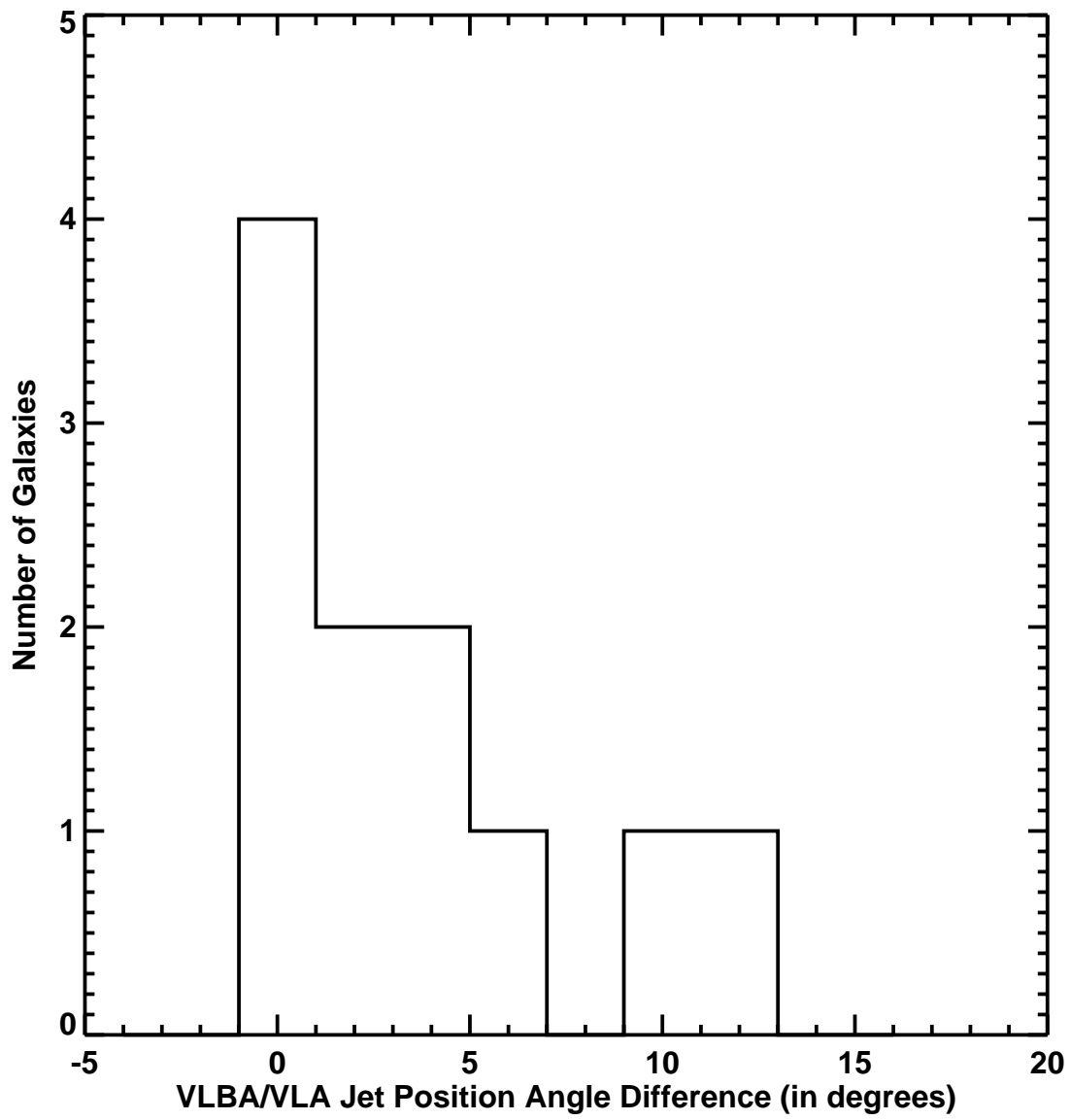


Fig. 2.—

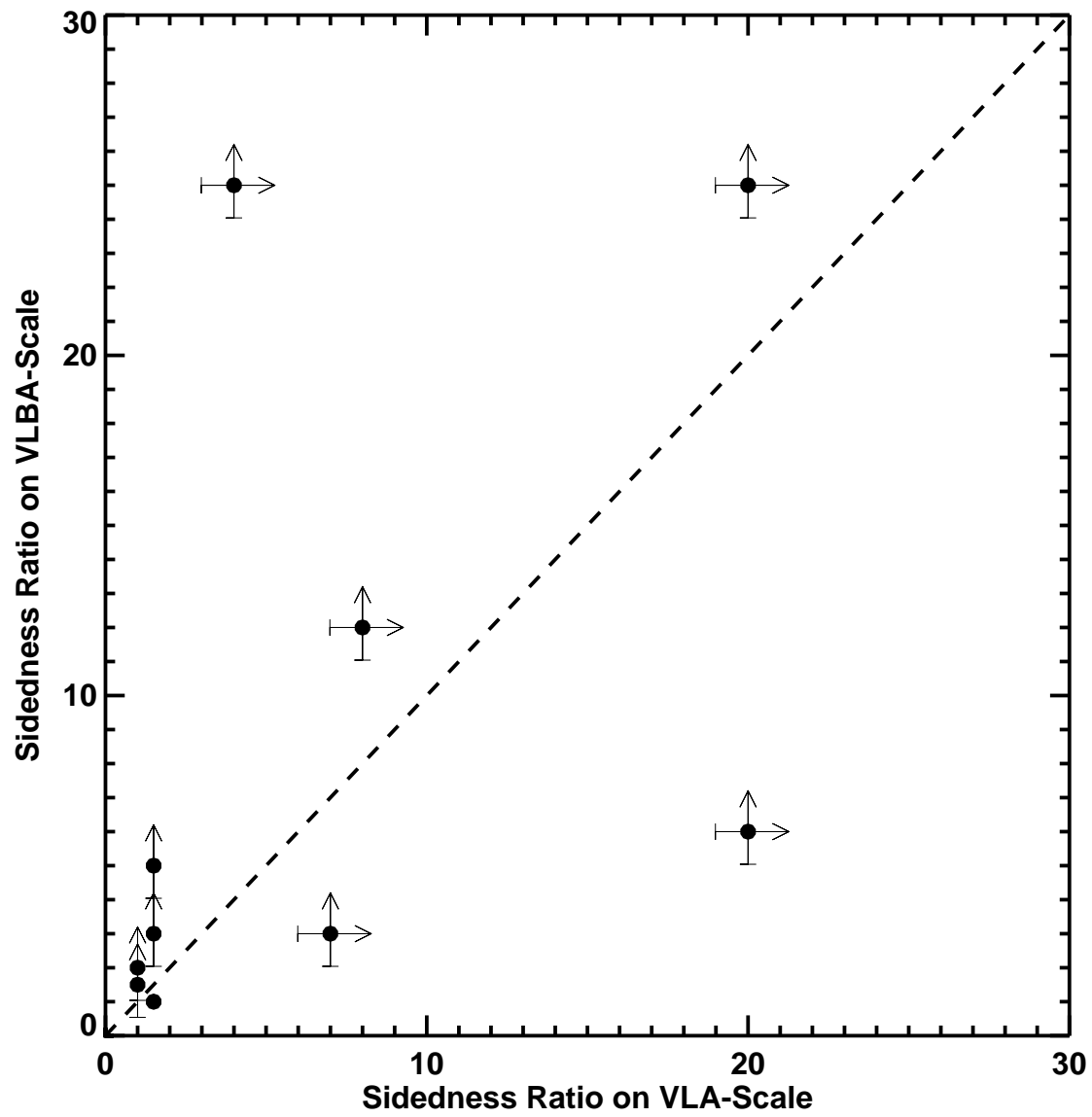


Fig. 3.—

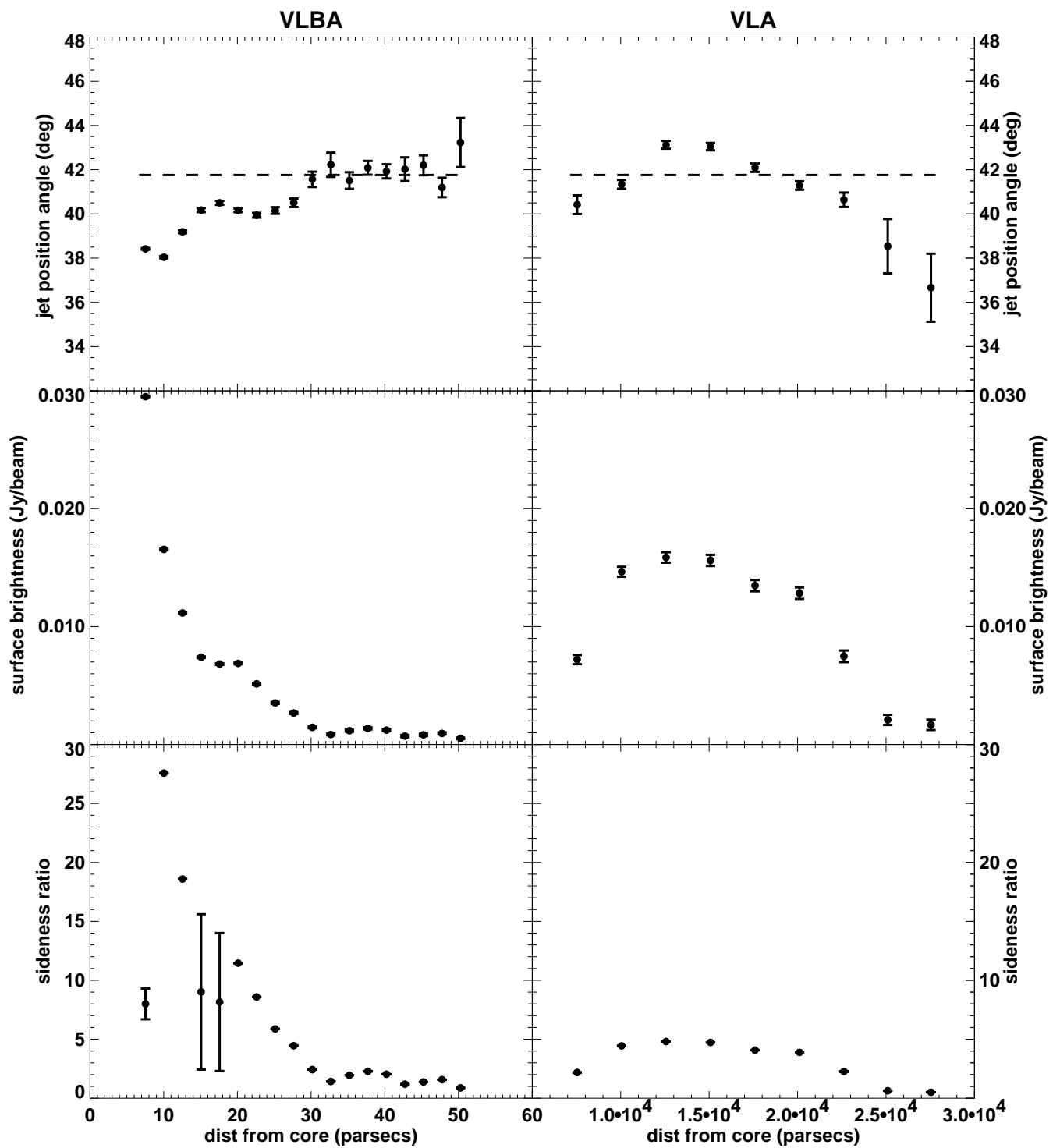


Fig. 4.—

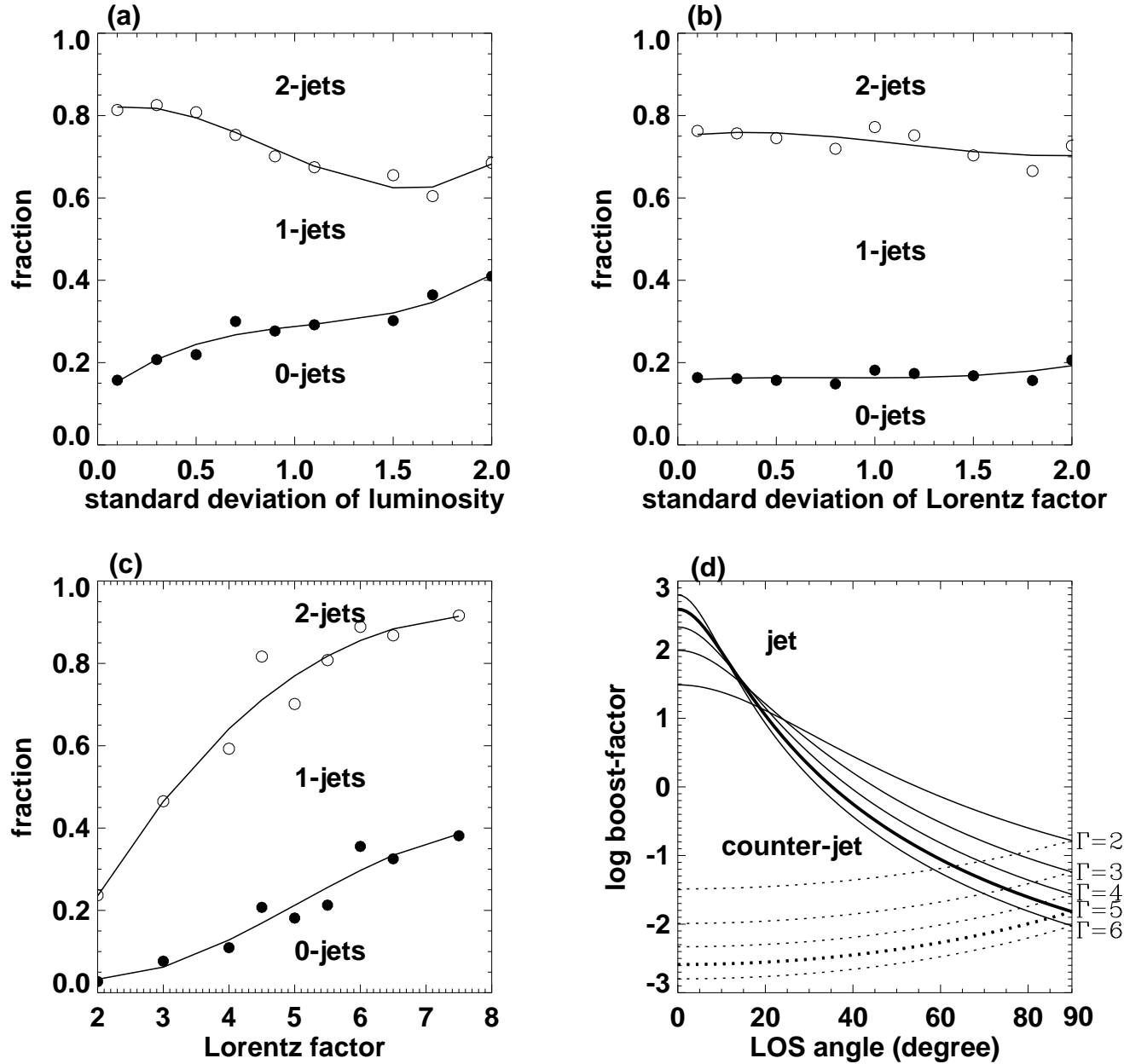


Fig. 5.—

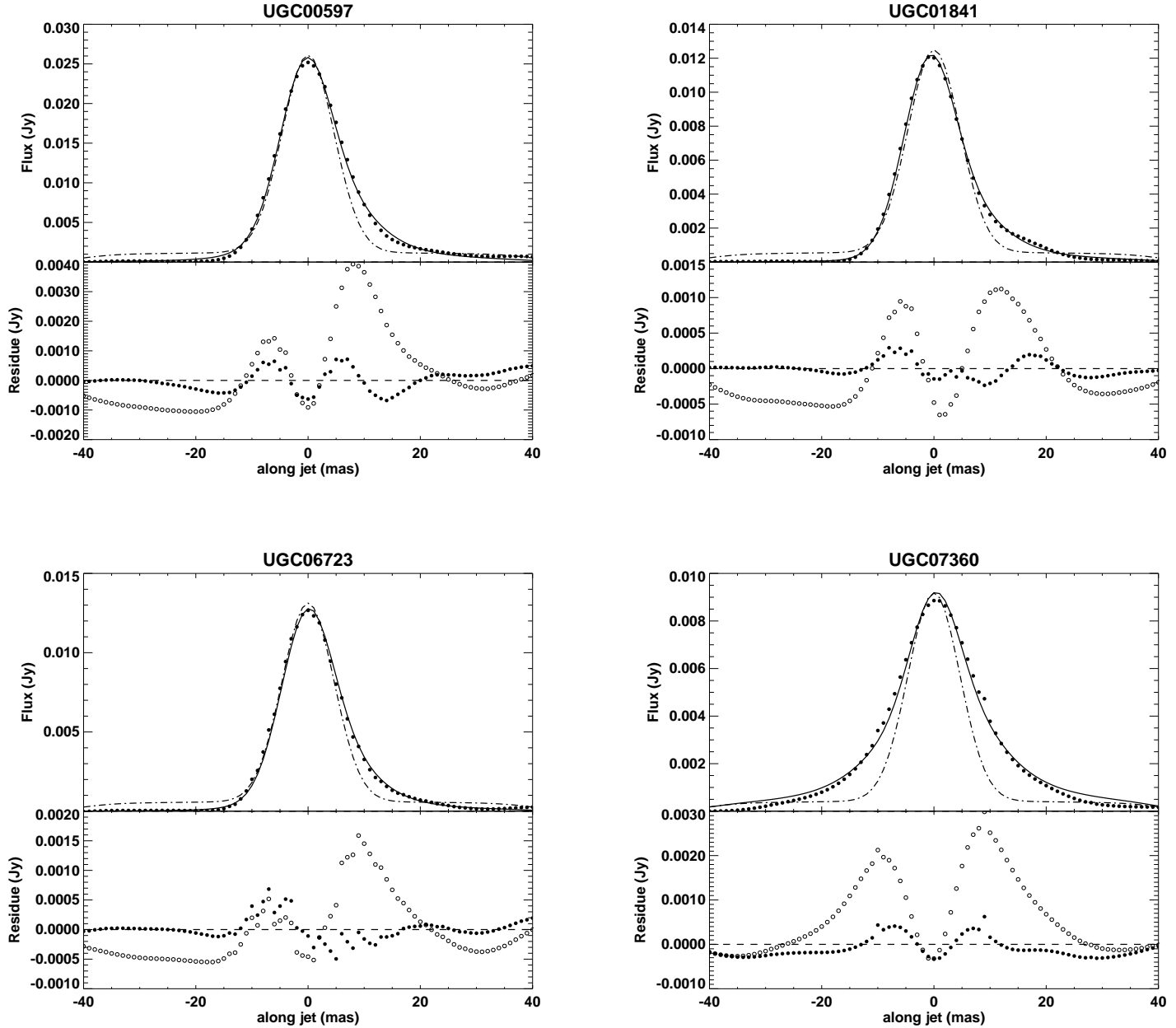


Fig. 6.—

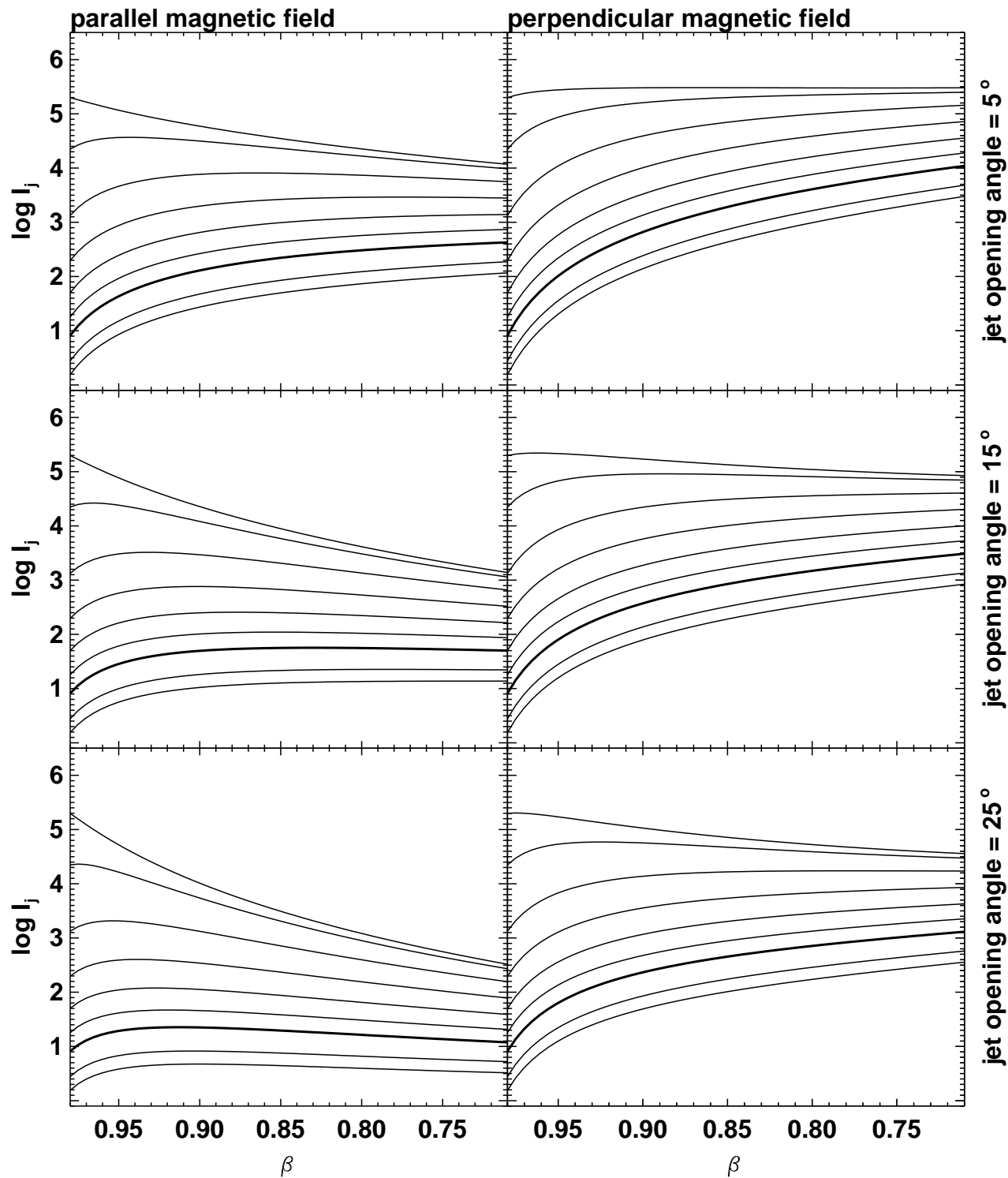


Fig. 7.—